INTERNATIONAL JOURNAL FOR NUMERICAL METHODS IN FLUIDS
Int. J. Numer. Meth. Fluids 2005; **47**:161–183
Published online 25 November 2004 in Wiley InterScience (www.interscience.wiley.com). DOI: 10.1002/fld.803

Fully implicit finite difference pseudo-spectral method for simulating high mobility-ratio miscible displacements

M. N. Islam and J. Azaiez*,†

Department of Chemical & Petroleum Engineering, University of Calgary, Calgary, Canada Alta. T2N 1N4

SUMMARY

A finite difference–pseudo-spectral (FD–PS) algorithm is developed to simulate the viscous fingering instability in high mobility-ratio (MR) miscible displacements. This novel algorithm uses the fully implicit alternating-direction implicit (ADI) method combined with a Hartley based pseudo-spectral method to solve the Poisson equation involving the streamfunction and the vorticity. In addition, under-relaxation in the iterative evaluation of the streamfunction is adopted. The new code allowed to model successfully the viscous fingering instability for mobility-ratios as high as 1800, and new non-linear viscous fingering mechanisms are discovered. A systematic analysis of the effects of the MR, the Peclet number and the aspect ratio on the finger growth is conducted. It is found that the growth of the interfacial instability accelerates with increase in the MR and Peclet number. At larger values of these parameters the increased stiffness of the corresponding numerical problem caused significant increase in the computational time as it required finer grids and smaller time steps to capture the fine structures of the viscous fingers. Copyright © 2004 John Wiley & Sons, Ltd.

KEY WORDS: viscous fingering; high MR; ADI method; non-linear simulation

1. INTRODUCTION

A flow process that involves the displacement of a fluid of a low mobility by another one of higher mobility leads to the development of an instability at the interface between the two fluids. This instability, known as viscous fingering, leads to the development of finger-shaped intrusions between the two fluids that affect the degree of mixing between the two phases. As a consequence, flow processes involving the displacement of one fluid by another and whose efficiency is determined by the degree of communication between the two fluids are

*Correspondence to: J. Azaiez, Department of Chemical & Petroleum Engineering, University of Calgary, Calgary, Canada Alta. T2N 1N4.
†E-mail: azaiez@ucalgary.ca

Contract/grant sponsor: Natural Sciences and Engineering Research Council of Canada (NSERC)
Contract/grant sponsor: Imperial Oil

Received 12 January 2004
Revised 27 September 2004

dependent on the severity of this instability. The major parameter that governs this instability is the mobility-ratio (MR) defined as the ratio of the mobility of the displacing fluid over that of the displaced one.

The objective of the present study is to investigate in a systematic way the nature of the instability that develops at the interface between two fluids in a high MR displacement process. Examples of processes that involve high MR displacements include the recovery of heavy oil and bitumen that has been gaining a lot of attention in the recent years. Given the large difference between the mobilities of the displaced and the displacing fluid, with the latter being much more mobile than the former, very complex fingering patterns develop at the interface between the two fluids. Features of viscous fingering of fluids can be studied conveniently in a Hele–Shaw cell since a single phase Hele–Shaw flow is analogous to two-dimensional incompressible flow in homogeneous porous media. Most of the earlier works has focused either on determining the conditions that lead to the onset of fingering or the non-linear evolution of viscous fingers at relatively small values of MR. However, in heavy oil and bitumen recovery processes, it is not sufficient to know whether or not instabilities will occur, since they can hardly be avoided. What is needed is a tool that is capable of predicting the displacement behaviour once the fingering has started. This study presents a numerical method that can simulate viscous fingering at high-MR miscible displacements involving Newtonian fluids in a rectilinear Hele–Shaw cell.

Efforts in the field of porous media flow simulation date back at least to the work by Peaceman *et al.* [1], who developed a FD algorithm for computing an unstable rectilinear miscible displacement. The authors employed the governing equations in their primitive formulation based on the velocity and pressure variables. Due to the low order of their numerical algorithm, a fingering instability did not develop on its own, but had to be triggered artificially by imposing small random spatial variation in the permeability. In this work the authors carried out simulation of viscous fingering for MRs up to 86 and validated their results by comparing them with the experiments of Blackwell *et al.* [2]. The spatial resolution they used (40×20 grids) was coarse and therefore unable to capture the initial growth of the fingering instability adequately.

Koval [3] and Todd *et al.* [4] developed empirical one-dimensional models to study viscous fingering in Newtonian displacements. Although their models predicted the evolution of the average concentration profile well, they suffered from major pitfalls. Indeed, such models failed to explain the mechanisms of the evolution of the instability, let alone predict the unstable flow. In a subsequent study, Fayers [5] attempted to remedy these failing by constructing an approximate one-dimensional model with adjustable parameters that can be physically interpreted. His adjustable parameters described a fingering function intended to mimic the two-dimensional geometry and depth averaged concentration field of an array of viscous fingers at any given time. The results were in good agreement with the experiments of Blackwell *et al.* [2]. Though the adjustable parameters of Fayers [5] now have physical meaning, his model still precludes a detailed explanation of the mechanisms whereby viscous fingers evolve.

Christie *et al.* [6] attempted to improve the FD scheme of Peaceman *et al.* [1] by using finer grids. They conducted simulations for longitudinal Peclet numbers as large as 2000 and MRs from 5 to 86 to model the experiments of Blackwell *et al.* [2]. All input data was taken from Blackwell's experiment and fingers were triggered by a random perturbation to the initial concentration. They found reasonable agreement between their calculations and the experimental prediction of the one-dimensional performance curve. In a subsequent study,

Christie [7] extended the previous work to coupled miscible and immiscible flows. This extension allowed the author to perform calculations when water and solvent flow simultaneously, and thus to calculate the stabilizing effects of a water alternate gas (WAG) scheme directly. In this work the author used 180×180 mesh and simulated viscous fingering for MRs up to 41 in rectilinear as well as quarter five spot geometry. In all the above numerical studies [1, 3–7], explicit schemes were used to solve the time-dependent concentration or saturation equations in a way that stability conditions were satisfied for the range of MRs used. These conventional FD methods are usually of second order overall accuracy, but often suffer from significant levels of numerical dispersion.

Considering the accuracy limitations of the grid based methods, several researchers have recently based their computational investigations on significantly more accurate Spectral methods [8–17]. Tan *et al*. [8] studied non-linear interactions of viscous fingers in miscible displacements in rectilinear Hele–Shaw cell, by carrying out simulations using Fourier transform based spectral method. Considering the case of isotropic dispersion, the authors were able to capture non-linear fingering mechanisms, such as *spreading*, *shielding* and *tip splitting* observed for the first time in their simulations. Zimmerman *et al.* [9] used Hartley transform based spectral method to extend the work of Tan *et al*. [8] in order to include the effects of anisotropic dispersion. They considered dispersion to be velocity dependent and studied the influence of anisotropy on the non-linear evolution of viscous fingers. A new fingering mechanism named *coalescence* was observed in their simulations for the first time. In a subsequent study, Zimmerman *et al*. [10] also observed *coalescence* mechanism in their isotropic simulation of viscous fingering at Peclet numbers as high as 4000. In another numerical investigation using spectral method, Tan *et al*. [11] studied the effects of the permeability heterogeneity. The authors found that the fingered zone grows linearly in time in a fashion analogous to that found in homogeneous media [8], indicating a close coupling between viscous fingering on the one hand and flow through preferentially more permeable paths, on the other. Zimmerman *et al.* [12] also carried out simulation of miscible displacements in a three-dimensional system and no new fingering mechanisms were observed. The authors concluded from the study that two-dimensional simulations are sufficient to capture the non-linear interactions of viscous fingers. More recently, Rogerson *et al*. [13] studied the effect of tangential shearing on non-linear evolution of viscous fingering, by including a tangential velocity component at the interface of a miscible flow displacement. The tangential shearing affected the shape and orientation of the fingers quite strongly and at the same time had influenced the wavelength and growth of the fingers. The authors observed new finger interaction mechanisms, such as *diagonal fingering* and *secondary side-fingering* instability, due to the presence of tangential shearing and gravity. In all these numerical investigations involving Spectral methods, the maximum value of MR studied was about 20. And in order to solve the time-dependent convection–diffusion equation for the concentration, either an explicit or a semi-implicit (predictor–corrector) algorithm was used.

A different line of research has aimed at implementing variants of the Finite Element method for studying viscous fingering in miscible displacements. Moissis *et al*. [18] used a Finite Element modified method of characteristics for solving the concentration equation and a mixed Finite Element scheme to solve the pressure equation. In this work a miscible flood of a rectangular slab was simulated in two spatial dimensions. The parameters that govern the flow were the viscosity ratio, Peclet numbers associated with molecular diffusion, longitudinal dispersion and transverse dispersion, and the aspect ratio of the slab. The effects of local

permeability variations and overall heterogeneity of the porous medium were also considered. The highest value of MR reached by Moissis *et al.* [18] was 750, but their results did not show interesting finger structures that were reported in studies at lower MRs using the finite difference [1, 3–7] as well as spectral methods [8–17]. This casts some doubts on the validity of their numerical algorithms and the results they reported. In a later study, Coutinho *et al.* [19] suggested that the combination of a finite element modified method of characteristics and a mixed finite element method leads to little numerical dispersion, allowing the use of large time steps and good accuracy in the computation of velocities. In their implementation of a parallel stabilized finite element technique, the governing equations were approximated in space by equal order elements. The resulting semi-discrete equations were approximated in time by a block-iterative predictor–multicorrector algorithm. Though the authors examined the effects of anisotropy and the non-monotonicity of the viscosity profile, they limited their investigation to low MR, only up to 20. More recently, Coutinho *et al.* [20] used stabilized finite element methods with reduced integration techniques for miscible displacement simulation in quarter five spot geometry. The authors reported that they were able to reach adverse MR as high as 1000, which to our knowledge, corresponds to the highest MR reported in the literature dealing with numerical simulation of the viscous fingering instability. The production curves at various MRs were compared with the results from a similar study by Castro *et al.* [21] and were found to be in good agreement. However, authors of these studies [20, 21] have not focused on identifying any new viscous fingering mechanism in such high MR miscible displacement simulations.

In another recent study, Meiburg *et al.* [22] implemented a compact FD discretization as well as a fully implicit alternating-direction implicit (ADI) algorithm to study homogeneous and heterogeneous miscible porous media flows. Following the works of Homsy and collaborators [8–12, 14, 15], the study was based on the streamfunction-vorticity formulation of Darcy's law and resolved all physically relevant length scales including diffusion. With a formal accuracy of $O(\Delta x^4, \Delta t^2)$, the numerical approach combined the ease of implementation and the ability to handle non-trivial geometries with the superior computational accuracy usually reserved for spectral methods. For numerical convenience the authors used the conservative form of the concentration equation while implementing the ADI method and the full time step Δt was split into two half steps of size $\Delta t/2$. During the first half step, the convection and diffusion terms in the x-direction were treated implicitly, while those in y-direction were dealt with explicitly. During the second half step, the roles were reversed. Though the authors considered their implementation of the ADI method to be fully implicit, the fact that the velocity field was frozen during the entire time step, i.e. all velocities were evaluated at the old time level, makes the algorithm in reality explicit. The authors were able to validate the code at an $\mathrm{MR} = 148.4$ using results of linear stability analysis, but did not show long time finger evolutions at such a large value of MR. Furthermore, only *side branching* (SB) instability was reported to as a new non-linear mechanism. To our knowledge, no similar study has been reported in the literature for $\mathrm{MR} = 148.4$ or higher that involves miscible displacement in a rectilinear geometry.

It can be seen from the above review that most previous studies were limited to low or moderate MRs ($\mathrm{MR} < 25$). Furthermore, to our best knowledge, the few studies that reached higher values, either suffered from numerical dispersion and therefore did not reveal interesting finger structures [18], or simply did not show the non-linear evolution of the fingers at the high-MR that the authors were able to reach [20–22]. In either case, the maximum MR did

not exceed 1000, which is below common values encountered in process involving adverse displacements such as the heavy oil recovery. As we shall see later, high MR displacements result in stiff problems that cause the code to diverge well before noticeable development of the physical instability at the interface. Hence, well adapted numerically stable algorithms are required to study the viscous fingering instability at higher MRs.

The objective of the present work is to develop a numerical algorithm that is well adapted for modelling the viscous fingering instability at high values of MR. From the series of non-linear simulations conducted using the adopted numerical tools, we will try to identify new non-linear viscous fingering mechanisms that dominate the flow at high-MR miscible displacements of Newtonian fluids involving isotropic dispersion. We will also investigate the effects of increase in the MR, Peclet number as well as aspect ratio (of the rectangular domain) on the dynamic evolution of the viscous fingers. This may allow us to analyse the mechanisms of instability at the interface involving very high viscosity contrast and the physics behind their development, which has not yet been examined quite explicitly in the literature.

In Section 2, we present the problem formulation and the governing equations. Section 3 deals with the numerical methods developed to solve the model problem, while Section 4 presents and discusses the non-linear simulation results. In Section 5, some conclusions will be drawn from this study.

2. PROBLEM FORMULATION

2.1. Physical problem

The pattern of the flow through porous media is complex and at the microscopic scale, not amenable to rigorous solution using fundamental laws of mass and momentum transport. A simplified and useful approach is to consider the fluid motion on a macroscopic scale while retaining the artifice of continuum. The macroscopic fluid properties and flow characteristics such as density, velocity and pressure, can still be thought of as point quantities and continuous. The well-known Darcy's law for flows through porous media is based on this approach. The two-dimensional Hele–Shaw flow uses the same macroscopic approach and has been used in a great wealth of literature for studying flow through porous media both experimentally and numerically.

A Hele–Shaw cell, which consists of two plane parallel plates each of dimensions L (length) and W (width)—placed close to each other making a thin gap $b \ll W$, is an analogue of a homogeneous porous medium of constant permeability k (see Figure 1). A two-dimensional miscible displacement in the gap between the two plates is considered, in which one fluid is displacing another. Both fluids are Newtonian and incompressible, and they are totally miscible. For a general case of a flow involving a fluid of viscosity μ_1 and density ρ_1 displacing another fluid of viscosity μ_2 and density ρ_2, an instability will develop at the interface between the two fluids if [23]

$$[(\mu_2 - \mu_1)U/k + (\rho_2 - \rho_1)g\cos\theta] > 0 \tag{1}$$

here, g is the gravitational acceleration, θ represents the angle between the plane and the z-axis, and U is the uniform velocity at which an incompressible fluid is injected from the left hand side. It can be easily seen from Equation (1) that a combination of unfavourable

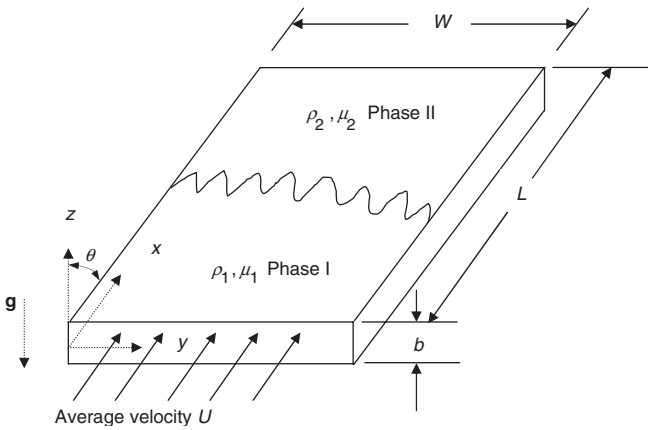

Figure 1. Schematic of a rectilinear Hele–Shaw flow system.

mobilities μ/k, and densities ρ of the two fluids will lead to an unstable flow displacement. In the present study, a horizontal rectilinear Hele–Shaw cell is considered ($\theta = \pi/2$) thus the effect of gravity is disregarded. Under this assumption, the instability is only driven by the viscosity difference between the two fluids.

Throughout this study the displacing fluid will be referred to as phase 1, while the displaced one will be denoted as phase 2. We will use a reference frame where the direction of the flow is along the x axis, the y axis is parallel to the initial plane of the interface while the z-axis is perpendicular to the plates.

2.2. Governing equations

The miscible displacement involving incompressible Newtonian fluids in a Hele–Shaw cell is described by the continuity equation, the momentum equation in the form of Darcy's law, and the convection–dispersion equation for the concentration of the displacing fluid c,

$$\nabla . \mathbf{u} = 0 \tag{2}$$

$$\nabla p = -\left(\frac{\mu}{k}\right)\mathbf{u} \tag{3}$$

$$\frac{\partial c}{\partial t} + \mathbf{u} \cdot \nabla c = \nabla \cdot (\underline{\underline{D}} \nabla c) \tag{4}$$

In the above equations, $\mathbf{u} = (u, v)$ is the velocity field, p the pressure, $\underline{\underline{D}}$ is the dispersion coefficient tensor and μ/k is the fluid mobility defined as the ratio of the viscosity μ and the permeability of the medium k. Here, we will consider the dispersion to be isotropic (i.e. $\underline{\underline{D}} = D\underline{\underline{I}}$), where D is assumed to be a constant. We will also assume that the viscosity is a general function of the concentration, $\mu = \mu(c)$.

2.3. Boundary and initial conditions

Once the model equations are found, we need to define the appropriate boundary and initial conditions to solve the model problem. Following previous studies [8–13, 15, 17, 22], we will implement periodic boundary conditions in the variables of the problem. Thus the physical boundary conditions are:

$$u(x=0,y,t)=U, \quad v(x=0,y,t)=0, \quad c(x=0,y,t)=c_1$$

$$u(x=L,y,t)=U, \quad v(x=L,y,t)=0, \quad c(x=L,y,t)=0 \tag{5}$$

$$(\mathbf{u},c)(x,y=0,t)=(\mathbf{u},c)(x,y=W,t) \tag{6}$$

Equations (5) deal with the streamwise direction, x. At the far left end, the concentration of phase 1 is $c_1=1$, while at the right edge, the concentration of phase 1 is zero since phase 2 is solvent free. The velocity of the fluids at the far-left and far-right ends is equal to the average injection velocity U.

Equation (6) represents periodicity in the transverse (y) direction in terms of concentration and velocity, but the x direction periodicity of the concentration poses a problem. One method to apply periodic conditions for the concentration in the x direction consists of doubling the domain size through a reflection at the right boundary $x=L$ [8, 9]. This method of doubling the domain makes the problem computationally more expensive. In a more efficient approach, first suggested by Manickam *et al.* [14] and successfully implemented in the work of Singh *et al.* [17], the total concentration at any time in space is split into two components—the solution of the one-dimensional convection–diffusion equation $\bar{c}(x,t)$ and a disturbance concentration, $c'(x,y,t)$:

$$c(x,y,t)=\bar{c}(x,t)+c'(x,y,t) \tag{7}$$

where, $\bar{c}(x,t)=1-\mathrm{erf}\left(x/\sqrt{4t}\right)/2$ and the expression for the disturbance concentration $c'(x,y,t)$ will be given when discussing the initial condition.

In this approach, one needs to solve the numerical problem only for the disturbance concentration c' instead of solving for the total concentration and then the total concentration can be obtained from Equation (7). The disturbance concentration c' is zero at both boundaries $x=0$, and L, which makes the concentration periodic in the x direction. The simulations will be stopped well before the fingers reach the other streamwise boundary. Thus the new periodic boundary conditions in the x direction can be presented as:

$$(\mathbf{u},c')(0,y,t)=(\mathbf{u},c')(L,y,t) \tag{8}$$

A constant linear velocity in the x direction and a given two-dimensional distribution of the solvent concentration are assumed at $t=t_0$, as appropriate initial conditions:

$$u=U, \quad v=0 \quad \forall(x,y)$$

at $t=t_0$:

$$c=c_0(x,y,t=t_0) \quad \forall(x,y) \tag{9}$$

Since the total concentration consists of the base state concentration and the disturbance term c'; either a random perturbation or a single wave of very small magnitude can be introduced

in the base state concentration at the initial interface. A mathematical description of the initial condition consists of the solution of the one-dimensional convection–diffusion equation and a random perturbation:

$$c_0(x, y, t = t_0) = \frac{1 - \mathrm{erf}\left(x/\sqrt{4t_0}\right)}{2} + \delta * \mathrm{rand}(y) * \exp(-x^2/\sigma^2) \tag{10}$$

where δ is the magnitude of the disturbance, rand is a random number between -1 and 1, σ is a parameter that determines the penetration of the disturbance from the front, erf represents the error function and t_0 is the initial time at which the perturbation concentration is added to the base state profile. The parameters δ, σ and t_0 all are small relative to unity, and the choice of their values determines the qualitative nature of the initial front. The use of random numbers as small perturbation allows the inclusion of the whole spectrum of wave numbers.

2.4. Scaling and basic equations

The equations are made dimensionless using diffusive scaling, thus diffusive length D/U and diffusive time D/U^2 are chosen for scaling the length and time variables, respectively. Since the permeability k of the medium is constant, it can be easily included in the viscosity itself. Letting the symbol μ represent the ratio μ/k, and referring to it henceforth as viscosity, the viscosities of the two fluids are scaled by the viscosity of the displacing fluid, μ_1. Finally, the pressure P is scaled by the characteristic pressure $\mu_1 D$ and the concentration by that of the displacing fluid so that it is equal to one in the displacing fluid and zero in the displaced one. Moreover, the flow is examined in a Lagrangian reference frame moving with a constant velocity U. At this moving reference frame the continuity equation, Darcy's law and the convection–dispersion equation take the following dimensionless forms:

$$\nabla.\mathbf{u}^* = 0 \tag{11}$$

$$\nabla P^* = -\mu^*(\mathbf{u}^* + \mathbf{i}) \tag{12}$$

$$\frac{\partial c^*}{\partial t^*} + \mathbf{u}^*.\nabla c^* = \nabla^2 c^* \tag{13}$$

In the above equations, $\mathbf{i}$ is the unit vector in the x-direction and the superscript $*$ is used to represent the dimensionless quantities. In all that follows the superscript $*$ will be dropped from the dimensionless parameters for convenience.

In practice, the viscosity–concentration relationship is complicated and changes with the choice of the fluids. However, we will assume a monotonic relationship between the viscosity and the concentration [8–13, 16, 17, 22] of the form

$$\mu(c) = \mathrm{e}^{R(1-c)} \quad \text{or,} \quad \frac{1}{\mu}\frac{\mathrm{d}\mu}{\mathrm{d}c} = -R \tag{14}$$

where R is defined as natural logarithm of MR or, $R = \ln(\mu_2/\mu_1) = \ln(\mathrm{MR})$. This particular choice for the relationship $\mu(c)$ is not restrictive, and any other viscosity–concentration relationship, such as quarter-power blending rule [15, 18, 24], can be easily implemented as well.

2.5. *Vorticity and streamfunction formulation*

For the purpose of solving the model equations numerically, we will follow earlier authors who have adopted a vorticity-streamfunction formulation to implement spectral methods [8–13, 15–17] as well as in some applications of FD and finite element methods [18, 22, 24]. The streamfunction and vorticity are related to the velocity field as follows:

$$u = \frac{\partial \psi}{\partial y}, \quad v = -\frac{\partial \psi}{\partial x} \tag{15}$$

$$\omega = \frac{\partial v}{\partial x} - \frac{\partial u}{\partial y} \tag{16}$$

The streamfunction ψ and the vorticity ω are related as

$$\nabla^2 \psi = -\omega \tag{17}$$

where ∇^2 is the Laplacian operator.

With the above formulation, the continuity equation is automatically satisfied, and the convection–dispersion equation (13) can be written as [9, 17]

$$\frac{\partial \bar{c}}{\partial t} + \frac{\partial c'}{\partial t} = -\left(\frac{\partial \psi}{\partial y}\left(\frac{\partial \bar{c}}{\partial x} + \frac{\partial c'}{\partial x}\right) - \frac{\partial \psi}{\partial x}\frac{\partial c'}{\partial y}\right) + \frac{\partial^2 \bar{c}}{\partial x^2} + \frac{\partial^2 c'}{\partial x^2} + \frac{\partial^2 c'}{\partial y^2} \tag{18}$$

In the above equation we have used the fact that the concentration is split into two components as shown in Equation (7). Since the base state concentration satisfies $\partial \bar{c}/\partial t = \partial^2 \bar{c}/\partial x^2$, the convection–dispersion equation for the disturbance concentration can be written as [9, 17]

$$\frac{\partial c'}{\partial t} = -J + \frac{\partial^2 c'}{\partial x^2} + \frac{\partial^2 c'}{\partial y^2} \tag{19}$$

where

$$J = \frac{\partial \psi}{\partial y}\left(\frac{\partial \bar{c}}{\partial x} + \frac{\partial c'}{\partial x}\right) - \frac{\partial \psi}{\partial x}\frac{\partial c'}{\partial y} \tag{20}$$

By taking the curl of Equation (12) and using the expression of the viscosity (Equation (14)), the pressure is eliminated and the following vorticity formation equation is obtained [8, 17]:

$$\omega = -RN \tag{21}$$

where

$$N = \frac{\partial \psi}{\partial x}\left(\frac{\partial \bar{c}}{\partial x} + \frac{\partial c'}{\partial x}\right) + \frac{\partial \psi}{\partial y}\frac{\partial c'}{\partial y} + \frac{\partial c'}{\partial y} \tag{22}$$

The boundary conditions in terms of perturbation concentration, streamfunction and vorticity can be written as

$$\text{Streamwise direction} \quad (\psi, \omega, c')(0, y, t) = (\psi, \omega, c')(Pe, y, t) \tag{23}$$

$$\text{Transverse direction} \quad (\psi, \omega, c')(x, 0, t) = (\psi, \omega, c')(x, Pe/A, t) \tag{24}$$

In the above equations, $Pe = LU/D$ is the Peclet number and $A = L/W$ is the cell aspect ratio.

3. NUMERICAL METHOD

In order to solve the model problem numerically for high MRs, we adopted two different computational approaches. In the first approach, a combination of pseudo-spectral and FD methods is applied. In this scheme, the equations are transformed into Hartley space using Hartley transform and then the resulting ordinary differential equation for the concentration is advanced in time. Semi-implicit time-stepping algorithms are used and it was found that at higher MR, numerical instability causes the code to diverge at very early stages of the finger evolution. As it will be discussed later, since it is difficult to implement fully implicit time-stepping algorithm with the spectral method, a finite difference based computational algorithm has been developed which solves the time-dependent convection–diffusion equation by means of a fully implicit ADI method. This algorithm combines the ease of implementation, the stability of a fully implicit time-stepping algorithm and the accuracy of the spectral method. Details of the implementation of this newly developed FD–PS algorithm is presented later in this section along with the convergence and validation tests.

3.1. *Pseudo-spectral (PS) method*

We have implemented a PS method based on the Hartley transform [9, 17, 25, 26]. The two-dimensional discrete Hartley transform (DHT) [25] for an arbitrary function of x and y can be given as

$$\hat{g}(k_x, k_y) = H[g(x, y)] = \frac{1}{\sqrt{N_x N_y}} \sum_{i=1}^{N_x} \sum_{j=1}^{N_y} g(x, y) \operatorname{cas}\left(\frac{2\pi k_x x}{N_x} + \frac{2\pi k_y y}{N_y} \right) \tag{25}$$

The above equation is a version of the DHT definition where the form of the transform and its inverse are the same. In this equation $\operatorname{cas} x = \cos x + \sin x$, k_x and k_y are the discrete wave numbers and N_x and N_y are the number of spectral modes in the x and y directions, respectively. It is worth mentioning that there can be different definitions for DHT. The derivatives of a function in the Hartley transform space can be easily derived from the transform of the function by using Hartley transform derivative theorems [26]. Further details of the method and its implementation to study the viscous fingering instability are found elsewhere [8–12, 17, 25–27]. The major advantage of this method is its high accuracy, often called spectral accuracy, where the order of accuracy depends only on the smoothness of the solution and the error decays exponentially for smooth functions. This is in contrast with the FD technique where the accuracy is fixed by the scheme. The Spectral method allows recasting the governing non-linear partial differential equations into a system of ordinary differential equations in time for the variables in the transform space. Then, the ordinary differential equations are stepped in time using explicit or semi-implicit predictor–corrector time-stepping algorithm. In particular, we have used Adams–Bashforth predictor of the first, second and third order with the corresponding Adams–Moulton corrector along with a diffusive–convective operator-splitting algorithm. To allow accuracy and stability in time-stepping, a correction evaluation sequence is used to make the method as semi-implicit as desired.

Our attempts to simulate viscous fingering using PS method with semi-implicit time-stepping algorithms often showed numerical instability for $\mathrm{MR} > 24.5$. We suspect that this is due to the fact that the predictor–corrector algorithms are only conditionally stable, which ultimately caused the code to diverge. However, implementing fully implicit unconditionally stable time-

stepping algorithms with the PS method is difficult due to the fact that the Hartley transform of the product of two functions is not equal to the product of the Hartley transforms of the functions involved. In the following part we discuss another alternative that combines the accuracy of the PS methods and the ability to implement fully implicit time-stepping algorithms.

3.2. Finite difference–pseudo-spectral (FD–PS) method

In this part, we used a fully implicit method based on the ADI technique, first introduced by Peaceman *et al.* [28]. Ferziger [29] showed that the ADI method is consistent, $O(\Delta t^2) + O(\Delta x^2) + O(\Delta y^2)$, and unconditionally stable. Meiburg *et al.* [22] used this method to study miscible displacement in five-spot geometry. Although the authors stated that they have implemented a fully implicit ADI scheme, it was found that in order to combine the high accuracy of the compact FD method [30] with the ADI scheme, they had to consider the velocity field frozen at the old time-point while stepping in time. This in fact makes the algorithm explicit and therefore conditionally stable.

In the present work, conventional FD method is used to retain the fully implicit nature of the ADI method. We also used a spectral module to determine the streamfunction from vorticity distribution by solving the Poisson equation. Thus in the proposed numerical algorithm, we successfully combined the stability of the ADI scheme and the high accuracy of the spectral method. As we shall see later, this new algorithm allows to reach high values of the MR.

In what follows, the FD–PS implementation of the ADI scheme will be discussed. We will also discuss the validation and convergence tests on the newly developed FD–PS algorithm.

3.2.1. Implementation of the FD–PS algorithm. In the implementation of FD–PS algorithm, the convection–diffusion equation (Equation (19)) and the vorticity formation equation (Equation (21)) are solved simultaneously, and the Poisson equation (Equation (17)) relating vorticity and streamfunction is used to obtain the streamfunction from the vorticity distribution. While solving the convection–diffusion equation (Equation (19)) using ADI scheme, both convective and diffusive terms are discretized with second order accuracy when implicit, and with spectral accuracy (using Hartley transform) when explicit. The right hand side of the vorticity equation (Equation (21)) is always determined with spectral accuracy. The elliptic Poisson equation for the determination of the streamfunction from the vorticity distribution is also solved using the fast Hartley transform. Once the streamfunction is determined, the velocity components are computed by differentiation in the Hartley space. Detailed description of the implementation of FD–PS ADI scheme will be given next, by explaining the two half steps ($\Delta t/2$) that comprise the complete step (Δt) in time advancement of the convection–diffusion equation. The following notations are considered for the time points:

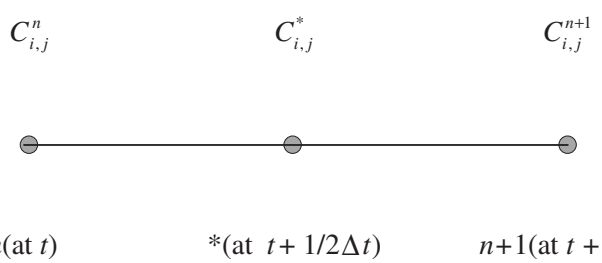

For time advancement from t to $t+1/2\Delta t$, taking implicit step in x direction and explicit step in y direction, and using second order centred difference formula for the spatial derivatives, the convection–diffusion equation (Equation (19)) results in the following semi-discrete set of equations:

$$\frac{c^*_{i,j}-c^n_{i,j}}{\Delta t/2}=-\left[\psi^n_{y(i,j)}\left(\bar{c}_{x(i,j)}+\frac{c^*_{i+1,j}-c^*_{i-1,j}}{2\Delta x}\right)-\psi^*_{x(i,j)}c^n_{y(i,j)}\right]+\frac{c^*_{i+1,j}-2c^*_{i,j}+c^*_{i-1,j}}{\Delta^2 x}+c^n_{yy(i,j)}$$

which can be rearranged as

$$c^*_{i-1,j}\left(\psi^n_{y(i,j)}\frac{1}{2\Delta x}+\frac{1}{\Delta^2 x}\right)+c^*_{i,j}\left(-\frac{2}{\Delta^2 x}-\frac{2}{\Delta t}\right)+c^*_{i+1,j}\left(-\psi^n_{y(i,j)}\frac{1}{2\Delta x}+\frac{1}{\Delta^2 x}\right)=\psi^n_{y(i,j)}\bar{c}_{x(i,j)}-\psi^*_{x(i,j)}c^n_{y(i,j)}-\frac{2c^n_{i,j}}{\Delta t}-c^n_{yy(i,j)} \tag{26}$$

Here, superscripts ^{n} and * denote evaluation at the previous and intermediate time levels, respectively. The explicit terms $\psi^n_{y(i,j)}$, $c^n_{y(i,j)}$ and $c^n_{yy(i,j)}$ are evaluated using the Hartley transform derivative theorem [9, 17, 25, 26]. For periodic boundary conditions the above discretization results in a cyclic tri-diagonal system of equations for $c^*_{i,j}$, where the value of $\psi^n_{x(i,j)}$ is used for $\psi^*_{x(i,j)}$ to evaluate the right hand side for the first time. The cyclic tri-diagonal system of linear equations is then solved block-wise, using Sherman–Morrison formula along with a band matrix solver. Once the value of $c^*_{i,j}$ is obtained, the vorticity formation equation (Equation (21)) as well as the vorticity–stream function relationship (Equation (17)) can be used to update $\psi^*_{i,j}$ and $\psi^*_{x(i,j)}$ values. Using this new value of $\psi^*_{x(i,j)}$ in Equation (26), iteration can be continued for $c^*_{i,j}$ until a certain relative convergence criterion is met. It is worth mentioning that Meiburg *et al.* [22] used the conservative form of equation (19) in their ADI scheme. They evaluated the term $uc|^*_{i,j}$ at the intermediate time step, then $c^*_{i,j}$ was obtained by dividing $uc|^*_{i,j}$ with $u^n_{i,j}$, which is considered frozen at the previous time step. This actually makes their algorithm not fully implicit. Whereas in our ADI scheme, both $c^*_{i,j}$ and $u^*_{i,j}$ terms are evaluated at the new time point, which makes the algorithm fully implicit in time.

The vorticity formation equation at the intermediate time level takes the form

$$\omega^*_{i,j}=-R[\psi^*_{x(i,j)}(\bar{c}_{x(i,j)}+c^*_{x(i,j)})+(\psi^n_{y(i,j)}+1)c^n_{y(i,j)}] \tag{27}$$

Typically the Poisson equation $\omega^*_{i,j}=-\psi^*_{xx(i,j)}-\psi^*_{yy(i,j)}$ is solved to obtain $\psi^*_{i,j}$ and with this value, $\psi^*_{x(i,j)}$ is determined. Then, $\omega^*_{i,j}$ is updated using Equation (27) and several iterations are carried out. Ruith *et al.* [16] suggested that some under-relaxed iteration in the streamfunction evaluation step can ensure quicker convergence at larger values of Pe and R. We used similar under-relaxation in our simulation and we continued iterating until the relative convergence criterion, for $\psi^*_{i,j}$, is met. It was observed that the value of the under-relaxation parameter ϖ has a strong influence on the convergence of the numerical code for MR greater than 24.5. Although there exists in the literature some standard expressions for the optimum value of

the over-relaxation parameter for some special problems, we had in this case to evaluate the optimum value of ϖ through trial and error. We set a limit to the number of iterations equals to 200, since it was observed that beyond this limit additional iterations do not improve the advancement of the numerical code.

For the second half step, we obtain the following semi-discrete set of equations from the convection–diffusion equation:

$$\frac{c_{i,j}^{n+1}-c_{i,j}^{*}}{\Delta t/2}=-\left[\psi_{y(i,j)}^{n+1}(\bar{c}_{x(i,j)}+c_{x(i,j)}^{*})-\psi_{x(i,j)}^{*}\frac{c_{i,j+1}^{n+1}-c_{i,j-1}^{n+1}}{2\Delta y}\right]+c_{xx(i,j)}^{*}+\frac{c_{i,j+1}^{n+1}-2c_{i,j}^{n+1}+c_{i,j-1}^{n+1}}{\Delta^{2}y}$$

which also can be rearranged as

$$c_{i,j-1}^{n+1}\left(-\psi_{x(i,j)}^{*}\frac{1}{2\Delta y}+\frac{1}{\Delta^{2}y}\right)+c_{i,j}^{n+1}\left(-\frac{2}{\Delta^{2}y}-\frac{2}{\Delta t}\right)+c_{i,j+1}^{n+1}\left(\psi_{x(i,j)}^{*}\frac{1}{2\Delta y}+\frac{1}{\Delta^{2}y}\right)=\psi_{y(i,j)}^{n+1}(\bar{c}_{x(i,j)}+c_{x(i,j)}^{*})-\frac{2c_{i,j}^{*}}{\Delta t}-c_{xx(i,j)}^{*}\tag{28}$$

and the following form of vorticity formation equation:

$$\omega_{i,j}^{n+1}=-R[\psi_{x(i,j)}^{*}(\bar{c}_{x(i,j)}+c_{x(i,j)}^{*})+(\psi_{y(i,j)}^{n+1}+1)c_{y(i,j)}^{n+1}]\tag{29}$$

A similar approach is taken to evaluate c^{n+1} and ψ^{n+1} values at time step $^{n+1}$. Thus it can be easily concluded that the formal accuracy of the algorithm is $O(\Delta x^{2},\Delta t^{2})$, although the explicit derivatives as well as the derivatives of c and ψ, while performing iteration are determined with spectral accuracy.

3.2.2. Validation of the FD–PS code. Rigorous validation represents an important step in establishing the accuracy and convergence properties of a new numerical algorithm. Thus, before conducting non-linear simulations with the newly developed FD–PS algorithm, we validated our numerical code by conducting some standard tests. In order to validate the complex coupling between concentration, viscosity and velocity fields, we carried out simulations for relatively small values of MR, for which there exist standard results published in the literature [8]. We also conducted other simulations with the original PS code that was used by Singh *et al.* [17], and compared the results in the form of concentration contours at various time levels of advancement. A systematic comparison of the magnitudes (L2 norm) of the concentration fields obtained by both FD–PS and PS codes was done to quantify the difference between the two results at the same time level. The relative tolerance was found to be of the order of 10^{-6}. These comparisons showed that the new algorithm is capable of simulating viscous fingering with comparable accuracy to the PS code.

We have also tested the convergence of the FD–PS code with mesh refinement, and conducted simulations using a single wave as initial perturbation with mesh resolutions of 64×64, 128×128, 256×256 and 512×512. Evaluation of the relative magnitudes of the concentration fields at successive increase in the spatial resolution showed that for 128×128 and 256×256

grids, the relative tolerance was of the order of 10^{-6}. On the other hand for 256×256 and 512×512 grids, the relative tolerance was found to be of the order of 10^{-8}. The contour plots for resolutions 256×256 and 512×512 also matched perfectly, which thus led to the conclusion that the code converges with grid refinement.

The above validation and convergence tests serve not only as a test for the proper coupling of concentration and velocity fields, but also as a check on the amount of artificial diffusion introduced by the discretization. Such numerical diffusion would result in an effectively lower value of Pe, which should affect the non-linear growth of the viscous fingers. The excellent agreement between the results generated by the FD–PS code and the PS code shows that the FD–PS discretization effectively prevents any problem related to numerical diffusion.

3.2.3. Effects of ϖ on the advancement of the FD–PS code. We carried out several tests on the effects of the under-relaxation parameter (ϖ) on the convergence of the numerical algorithm at high MR. Unless otherwise mentioned, typical values of the parameters were set as: $Pe = 500$, $A = 1$, $t_0 = 0.5$, $\sigma = \delta = 0.01$ and the relative tolerance was set to 10^{-4}. In this part of the study, we investigated the effect of the under-relaxation parameter on the viscous fingering instability, while varying the spatial resolution as well as the time step size whenever necessary. We set the starting point for MR to be 27 since the PS code could successfully simulate non-linear viscous fingers for MR up to 24.5. Table I gives a summary of this study as well as the progress attained.

An analysis of the results given in Table I reveals that the underrelaxation parameter ϖ has a strong influence on the convergence and stability of the numerical code. The under-relaxed iteration in the streamfunction evaluation from the vorticity using $\varpi = 0.8$ allowed to reach an MR $= 49.4$ which is larger than the maximum value obtained with the original PS code. A larger value, MR $= 164$ was attained by decreasing ϖ to 0.5, however further decrease in ϖ to 0.4 did not allow to reach larger values of the MR when using 128×128 grids. Using the same resolution and $\varpi = 0.4$, a decrease in the time step size dt from 5×10^{-3} to 5×10^{-4} did not lead to any improvement either. On the other hand increasing the spatial resolution to 256×256 pushed the limit in MR to 544.6. For later simulations, 256×256 or higher number of grids was used. By further decreasing the value of ϖ to 0.3 and dt to 2.5×10^{-4}, we were able to simulate successfully the viscous fingering instability up to MR $= 1096.6$ at $Pe = 500$. The highest mobility ratio reached with the new code is MR $= 1808$ for a Peclet number of 250.

Table I. Effects of ϖ on simulation advancement for $Pe = 500$.

Number of grid points	Step size, dt	ϖ	MR
256×256	5×10^{-3}	0.8	44.7
128×128	5×10^{-3}	0.8	49.4
128×128	5×10^{-3}	0.7	73.7
128×128	5×10^{-3}	0.6	134.3
128×128	5×10^{-3}	0.5	164.0
256×256	5×10^{-3}	0.4	544.6
256×256	2.5×10^{-4}	0.3	1096.6

Since it turned out that the under-relaxation parameter (ϖ) has a strong influence on the time advancement of the numerically stable FD–PS code for simulating viscous fingering at high MR, we revisited the PS code and implemented the under-relaxation in streamfunction evaluation step there. It was found that ϖ has similar influence on the advancement of the PS code at higher MR.

4. RESULTS

In this section, we will present the results of our numerical studies on high mobility-ratio miscible displacements. It needs to be mentioned that Compaq AlphaStation DS10 600 MHz workstations were used for all the simulations presented here. We will first identify and discuss new viscous fingering mechanisms that develop at high MR, and that as far as the authors' knowledge, are reported here for the first time. We will also discuss the effects of varying the MR, the Peclet number and the aspect ratio on the non-linear evolution of viscous fingers for random perturbation initial condition.

For all the simulations discussed in this part we set the parameters as follows: time step size $\mathrm{d}t = Pe \times 10^{-5}$, the spatial resolution 512×512 grids and relative tolerance for the convergence test $\mathrm{tol} = 10^{-4}$. The value of under-relaxation parameter ϖ varied with the mobility-ratio as discussed in the previous section (see Table I). The dimensionless time t_0 at which the perturbation is added to the interface is set to 0.5. In order to explain non-linear interactions of the viscous fingers, concentration contours between 0.1 and 0.8 are presented, with typical increment of 0.1. It is worth mentioning that, for aspect ratio of 2 or more, two periods in the y-direction is shown to capture the complete evolution of the fingers patterns.

4.1. Newly observed mechanisms

In this section new finger evolution mechanisms that are reported for the first time in simulations of miscible displacements of Newtonian fluids involving isotropic dispersion, will be discussed. Attempts are taken to use the terminology that describes best the whole non-linear mechanisms for all newly reported mechanisms.

In order to identify the new mechanisms that become dominant at large values of MR, the concentration contours shown in Figures 2–5 will be closely followed. Figure 2 shows a case

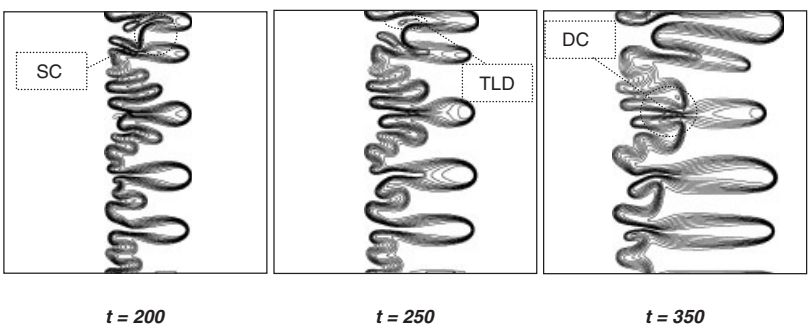

Figure 2. Concentration contours for $\mathrm{MR} = 148.41$, $Pe = 1000$ and $A = 1$.

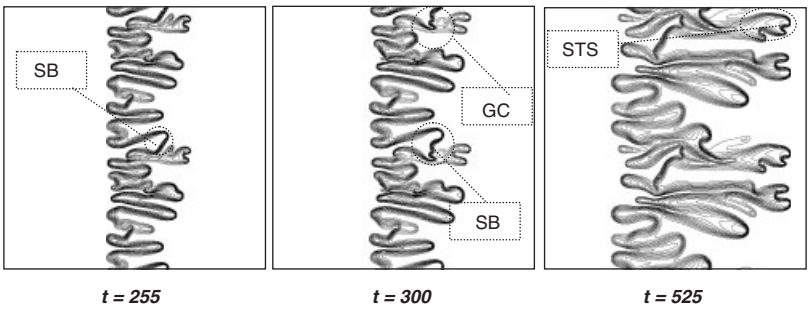

Figure 3. Concentration contours for MR = 148.41, $Pe = 1500$ and $A = 2$.

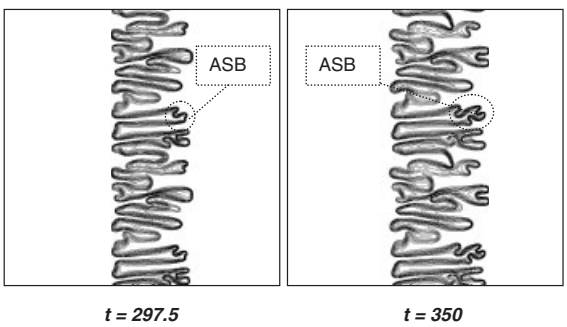

Figure 4. Concentration contours for MR = 148.41, $Pe = 1750$ and $A = 2$.

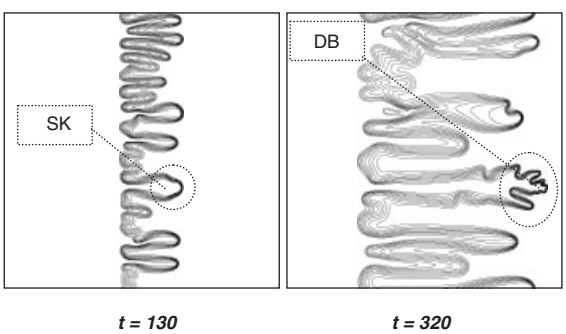

Figure 5. Concentration contours for MR = 403.43, $Pe = 1000$, and $A = 1$.

of MR = 148.41, $A = 1$ and for $Pe = 1000$; Figures 3 and 4 show two cases for MR = 148.41, $A = 2$ and for $Pe = 1500$ and 1750, respectively, whereas Figure 5 represents a simulation for MR = 403.43, $A = 1$ and $Pe = 1000$. It is worth mentioning that the simulations for MR values up to 403.43 covered all the newly observed viscous fingering mechanisms and no new mechanisms could be seen at higher MR. For brevity, the time sequences are not presented at the same time intervals, and only the frames that reveal new mechanisms are shown.

Stretched coalescence (SC): This very interesting coalescing mechanism is often observed in the shielded fingers at high mobility-ratios. As it can be seen in Figure 2 [frame, $t = 200$], the front of the circled finger stretches in the 'upward' direction and starts coalescing with the upper finger, whereas the lower front part of the coalescing finger does not follow the main flow direction and coalesces separately by stretching its way to the finger next to it. We have named this mechanism SC.

Trailing lobe detachment (TLD): Due to non-linear interaction between evolving fingers, sometimes a long trailing lobe of more viscous fluid forms which eventually detach from the interacting fingers (frame [$t = 250$] of Figure 2). This blob of the more viscous fluid then gets diffused in the less viscous displacing fluid with time. This mechanism was first observed in non-linear simulation of viscous fingering by Rogerson *et al.* [13] using tangential velocity component and was termed as TLD. It is reported for the first time in simulations involving miscible displacement of Newtonian fluids, without any tangential shearing.

Double coalescence (DC): In DC, two shielded fingers adjacent to a shielding finger bend into its base, and slowly merge into it. Frames [$t = 350$] of Figure 2, represent an excellent example of double coalescence. This interesting mechanism was first observed by Singh *et al.* [17] for miscible displacements involving non-Newtonian shear-thinning fluids, and was named DC. However, this is the first time such a mechanism is reported for a purely Newtonian miscible displacement.

Side branching (SB): The peculiarity of this mechanism is that the tips of the SB fingers are not directed in the streamwise direction but are directed slightly 'upward' or 'downward'. This movement of the tips generates shear in two different directions, making the concentration gradients steeper on the lower side of the upward directed finger and on the upper side of the downward directed finger. The circled finger in frame [$t = 255$] of Figure 3 initially evolves through a shielding mechanism and grows in an inclined fashion while competing with its neighbours. Later at $t = 300$, instabilities grow on the lower side of this inclined finger. As the instabilities on the side of the finger grow, in usual case the fingerlets continue to grow and split, resulting in SB instability. The SB instability was also reported by Singh *et al.* [17] in their simulations involving non-Newtonian shear-thinning fluids. To the author's knowledge, this is the first time it is observed for a Newtonian miscible displacement.

Gradual coalescence (GC): In a conventional coalescence mechanism, the tip of the coalescing finger bends and merges into the neighbouring shielding finger. Here we identified a new coalescing mechanism in which the slightly inclined shielding finger gradually merges into its closest neighbour through the fingerlets developed on the inner side of the finger. We named this interesting mechanism GC (see frame $t = 300$ of Figure 3). To our knowledge, GC is reported for the first time in the present study.

Single-sided tip-splitting (STS): In a typical TS mechanism, the streamwise directed shielding finger spreads at the tip and splits into two even fingerlets [9]. At the initial stage of the current mechanism, the tip of the finger splits unevenly. The wider part of the finger then spreads and goes through another tip-splitting mechanism, and the process continues. We named this mechanism as STS as the tip of the spreading finger splits in such a way that the thinner fingerlets always evolve in the same side of the parent finger. Frame [$t = 525$] of Figure 3 shows an excellent example of STS. This interesting mechanism is also observed for the first time in the present study.

Alternating side-branching (ASB): This is the most intriguing viscous fingering mechanism observed in our simulation. If we closely follow the evolution of the circled finger in Figure 4,

it can be easily seen that the branches are developing alternately on the upper and lower side of the stream-wise directed finger, and the major flow of the low viscosity fluid follows a spiral path. We named this mechanism ASB which, to our knowledge has not been reported in any previous study.

Skewering (SK): The shielding finger shown in frame [$t = 130$] of Figure 5 develops in a very unusual fashion which gives rise to a new fingering mechanism. The finger spreads first at the tip and in further development, the tip does not go through any kind of tip-splitting instability—a small bump grows at the middle of the tip instead. This interesting mechanism was referred to as SK in literature. SK was reported by Kawaguchi *et al.* [31] in the immiscible displacement at very high injection rate and was also seen in miscible displacement experiments of non-Newtonian fluids [32]. However, this is the first time a numerical simulation of a Newtonian flow displacement reveals this mechanism.

Dense branching (DB): The small bump described previously (frame [$t = 130$] of Figure 5) grows with time and evolves via TS and other non-linear mechanisms. In further development of the finger into the more viscous fluid ([$t = 320$] of Figure 5), the numerous side branches evolve so close to each other that the growth mechanism can be referred as DB. Li [32] observed DB mechanism in his miscible displacement experiments involving shear-thinning fluid. However, DB is reported for the first time for displacements of Newtonian fluids in our simulation.

4.2. *Effects of MR at high MR miscible displacements*

In this section, the effect of increasing MR is studied while fixing all other parameters including the Peclet number. We adjusted the value of the under-relaxation parameter ϖ following the previous discussion. We conducted three simulations for three large values of the MR, MR = 148.41, 403.43 and 1096.63. The dimensionless flow rate Pe was set to 750 while the aspect ratio was set to 1. Table II summarizes the time advancement for all these simulations as well as the corresponding computational times. In the table, t_{advanced} represents the dimensionless time required by the viscous fingers to reach the stream-wise boundary of the cell. A quick review of Table II shows that the computational time increased quite significantly with increase in MR. This apparent slow down of the code may be due to the increased instability in the physical process with increase in MR, which also made the corresponding numerical problem a stiff one at higher levels of time. However, at larger values of MR the increased stiffness of the corresponding numerical problem could be resolved by using finer grids and smaller time steps to capture fine structures of the viscous fingers.

Few contour plots are shown in Figures 6(a) and (b) to illustrate the effect of increase in the mobility ratio on the finger structures. It is clear that the complexity of the viscous fingering mechanisms increases quite significantly with the increase in MR. Besides *spreading*,

Table II. Effect of mobility ratio using random noise perturbation ($Pe = 750$, $A = 1$).

MR	ϖ	t_{advanced}	Computational time (hh:mm:ss)
148.41	0.5	322.5+	178:41:02
403.43	0.4	262.5+	274:12:02
1096.63	0.3	217.5+	292:11:19

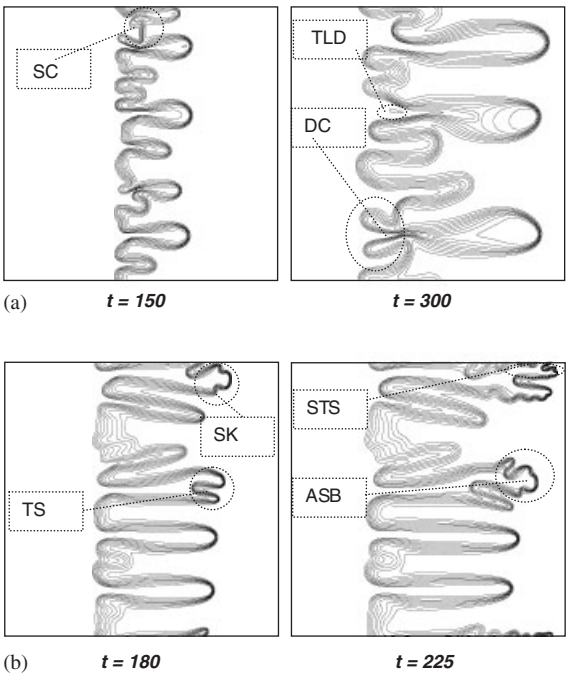

Figure 6. Concentration contours for $Pe = 750$, $A = 1$ and (a) MR = 148.41, (b) MR = 1096.63.

shielding, *fading* and *coalescence*, the major viscous fingering mechanisms observed are: SC, DC and TLD at MR = 148.41; and SK, TS, STS and ASB at MR = 1096.63.

From the type of viscous fingering structures observed at higher MR, the increased influence of viscous cross flow with increase in MR can be easily traced.

4.3. *Effects of Peclet number* (Pe) *at high MR*

From the definition of Peclet number, a higher value of Pe either means lower level of diffusion (D) for fixed flow rate (U) of the displacing fluid, or larger flow rate at fixed level of diffusion. However, for a given combination of fluids the value of Pe is directly proportional to the flow rate. Small flow rates provide diffusion with enough time to smear out the concentration field, whereas for larger flow rates steeper concentration gradients can be maintained. In this part of the study, the effects of Peclet number (Pe) at high MR on the development of the viscous fingering instability in miscible displacements is studied systematically. The value of Pe is varied as 750, 1000 and 1250 while fixing $A = 1$ and MR = 148.41. The time advancements of the simulations are summarized in Table III and the appropriate contour plots are shown in Figures 6(a), 2 and 7.

It should be stressed at this point that in diffusive scaling the length of the computational domain is $Lx^* = Pe$. Thus, from Table III it can be easily seen that the increase in Pe accelerates the evolution of the interfacial instability, such that the fingered front reaches the boundary faster. The non-linear mechanisms observed at $Pe = 750$ are already discussed in previous section and shown in Figure 6(a). It can be seen from Figure 2 that at $Pe = 1000$, the

Table III. Effects of Peclet number for MR = 148.41 and $A = 1$.

Pe	ϖ	t_{advanced}	Computational time (hh:mm:ss)
750	0.5	322.5+	178:41:02
1000	0.5	400+	216:12:45
1250	0.5	400+	191:05:50

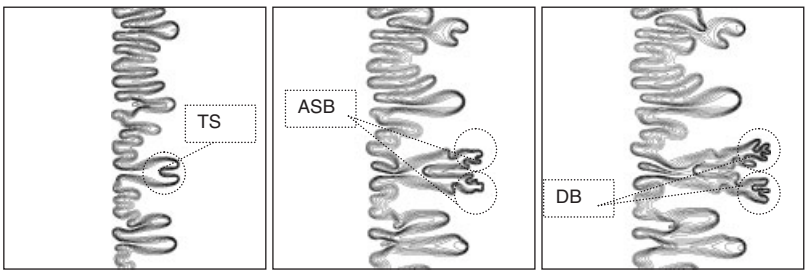

Figure 7. Concentration contours for MR = 148.41, $A = 1$ and $Pe = 1250$.

prevailing viscous fingering mechanisms are SC, TLD and DC. On the other hand, the contour plots shown in Figure 7 for $Pe = 1250$ present some very interesting fingering patterns. At this high value of Peclet number, TS instability occurs at a very early stage (Figure 7; frame [$t = 187.5$]). The finger that has gone through TS mechanism later shows ASB instability in each of its fingerlets. Finally, DB instability is seen to occur at the tip of the fingerlets.

From the parametric study shown above, it can be concluded that an increase in Pe results in more complex viscous fingering patterns and stronger competitions among the evolving fingers. Thus at high Peclet numbers, the non-linear interactions of the competing fingers cause a number of new and interesting fingering mechanisms to flourish in high mobility ratio miscible displacements. What we also observed by varying spatial and temporal resolution is that finer resolution and smaller time steps are required to capture the fine finger structures at larger Peclet numbers.

4.4. *Effects of aspect ratio* (A) *at high mobility-ratios*

The aspect ratio ($A = L/W$) of the computational domain is another important parameter that influences the number of fingers as well as their growth mechanisms. Recalling that the dimensionless streamwise length is $Lx^* = Pe$ and the dimensionless transverse length is $Ly^* = A$. Pe, one sees that by varying the aspect ratio of the domain, the transverse length available for non-linear interactions can be altered. In order to investigate the effects of A on the non-linear evolution of viscous fingers, we carried out three simulations for aspect ratios of 2, 4 and 8, with a relatively large value of the MR (MR = 148.41) and a Peclet number $Pe = 1000$. Illustrative contour plots for this investigation are shown in Figures 8(a) and (b).

A close examination of the contour plots shown in Figure 8 reveals that $A = 4$ generates intricate viscous fingering structures, and that the finger structures become less complex with increasing aspect ratio. In particular for $A = 4$, the TS instability that occurred earlier

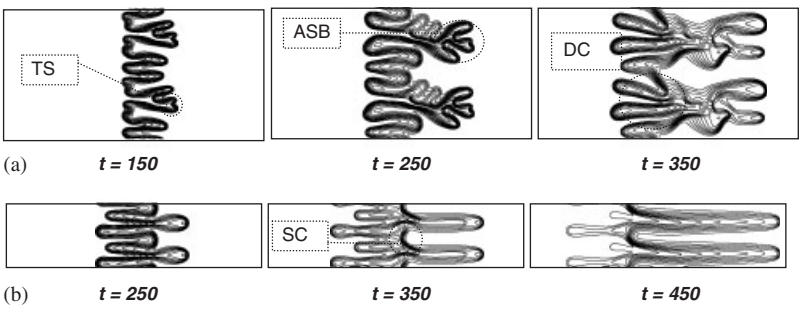

Figure 8. Concentration contours for MR = 148.41, $Pe = 1000$ and (a) $A = 4$, (b) 8.

Table IV. Effects of aspect ratio for MR = 148.41 and $Pe = 1000$.

A	ϖ	t_{advanced}	Computational time (hh:mm:ss)
2.00	0.5	390+	53:16:02
4.00	0.5	450+	57:11:19
8.00	0.5	630+	67:01:02

(Figure 8(a); frame [$t = 150$]) initiates ASB fingers. In later stages, as a result of DC of the neighbouring fingers to the alternating side branching finger, two of the alternate branches grow in the streamwise direction leading to a pair of fingers. At a larger aspect ratio of $A = 8$, the lack of sufficient length scale in the transverse direction is seen to induce mutual interaction of the spreading and shielding fingers which eventually results in a single dominant finger (shown in Figure 8(b)).

The decrease in the complexity of the finger structures with increasing aspect ratio can be explained by the reduction of the transverse length scale required for non-linear interaction of the viscous fingers. When the transverse length scale is reduced, the closely spaced fingers go through interplay of coalescence, fading and tip-splitting as well as other non-linear viscous fingering mechanisms. This eventually reduces the number of fingers to long time single dominant finger. On the other hand, a smaller aspect ratio provides larger transverse length scale for the non-linear interaction. At larger transverse length scale, increased non-linear interactions of viscous fingers often result in more complex structures.

A summary of the simulation advancement for $A = 2$, 4 and 8 is shown in Table IV. It is clear that the dimensionless time (t_{advanced}) required by the viscous fingers to reach the stream-wise boundary increases with increasing aspect ratio. This may be explained using the previous observations. Indeed, the interface consisting of a single finger ($A = 8$) is found to be less unstable than that with many intricate fingers at aspect ratio $A = 4$, and therefore it takes longer time for the fingered front to reach the stream-wise boundary at higher aspect ratio.

5. CONCLUSIONS

The objective of the present study is to develop a numerical algorithm that allows to model miscible flow displacement of Newtonian fluids at adverse MR. To this end, the flow has

been analysed using a rectilinear Hele–Shaw cell geometry, and a novel numerically stable algorithm has been developed.

The new numerical scheme combines both the FD and the spectral methods. The FD method allows implementing a fully implicit alternating-direction implicit (ADI) time stepping algorithm, while the PS method is used to solve the Poisson equation involving streamfunction and vorticity. In addition, underrelaxation is used while iterating to evaluate the streamfunction from vorticity-formation equation. It is found that the underrelaxation has a very strong effect on the convergence of the numerical algorithm at high MR. The newly developed FD–PS code allows simulating the non-linear viscous fingering with high accuracy for a MR as high as 1808, a value much larger than what has been reported so far in the literature.

Non-linear interactions of the viscous fingers are investigated at moderate–high MR. Finger interaction mechanisms reported by previous researchers in the case of Newtonian displacements at low–moderate MR ($MR \leqslant 20.1$), are all observed in our simulations. At high MR ($MR \geqslant 148.41$) new interesting viscous fingering mechanisms are observed. These mechanisms include SC, GC, STS, ASB, DB, SK, DC, TLD and SB. In particular, we think that the mechanisms of SB, ASB, STS and DB observed at high MR and sufficiently large Peclet numbers, are reminiscent of fractal structures, and may represent the viscous fingering structures observed in asymptotically high MR displacements. We have also analysed the effects of different parameters on the finger structures. As expected, an increase in the MR always causes increased instability at the miscible interface which results in new and interesting fingering mechanisms. Besides, an increase in the Peclet number also causes increased instability. Finally, it is found that smaller aspect ratios result in more complex finger structures.

Finally, we would like to comment that the new viscous fingering mechanisms reported here are observed using both PS and FD–PS algorithms and some of these mechanisms have experimental support in the literature. However, new independent computations or new laboratory experiments should be conducted to further validate the findings of this study.

ACKNOWLEDGEMENTS

The authors acknowledge the Natural Sciences and Engineering Research Council of Canada (NSERC) and Imperial Oil for the financial support of this project and MACI cluster at University of Calgary for computational resources.

REFERENCES

1. Peaceman DW, Rachford Jr HH. Numerical calculation multidimensional miscible displacement. *Society of Petroleum Engineers Journal* 1962; **2**:327–339.
2. Blackwell RJ, Rayne JR, Terry WM. Factors influencing the efficiency of miscible displacement. *Transactions of AIME* 1959; **216**:1–8.
3. Koval EJ. A method for predicting the performance of unstable miscible displacement in heterogeneous media. *Society of Petroleum Engineers Journal* 1963; 145–154.
4. Todd MR, Longstaff WJ. The development, testing, and application of a numerical simulator for predicting miscible flood performance. *Journal of Petroleum Technology* 1972; 874–882.
5. Fayers FJ. Approximate model with physically interpretable parameters for representing miscible viscous fingering. *Society of Petroleum Engineers Reservoir Engineering* 1988; **3**:5515–5558.
6. Christie MA, Bond DJ. Detailed simulation of unstable processes in miscible flooding. *Society of Petroleum Engineers Reservoir Engineering* 1987; **2**:514–522.
7. Christie MA. High-resolution simulation of unstable flows in porous media. *Society of Petroleum Engineers Reservoir Engineering* 1989; **4**:297–303.

8. Tan CT, Homsy GM. Simulation of non-linear viscous fingering in miscible displacement. *Physics of Fluids* 1988; **31**(6):1330–1338.
9. Zimmermann WB, Homsy GM. Nonlinear viscous fingering in miscible displacement with anisotropic dispersion. *Physics of Fluids A* 1991; **4**:1859–1872.
10. Zimmermann WB, Homsy GM. Viscous fingering in miscible displacements: Unification of effects of viscosity contrast, anisotropic dispersion and velocity dependence of dispersion on non-linear finger propagation. *Physics of Fluids A* 1992; **4**:2348–2359.
11. Tan CT, Homsy GM. Viscous fingering with permeability heterogeneity. *Physics of Fluids A* 1992; **4**(6): 1099–1101.
12. Zimmermann WB, Homsy GM. Three-dimensional viscous fingering: a numerical study. *Physics of Fluids A* 1992; **4**:1901–1914.
13. Rogerson A, Meiburg E. Numerical simulation of miscible displacement processes in porous media flows under gravity. *Physics of Fluids A* 1993; **5**:2644–2660.
14. Manickam O, Homsy GM. Stability of miscible displacements in porous media with nonmonotonic viscosity profiles. *Physics of Fluids A* 1993; **5**:1356–1367.
15. Manickam O, Homsy GM. Fingering instabilities in vertical miscible displacement flows in porous media. *Journal of Fluid Mechanics* 1995; **288**:75–102.
16. Ruith M, Meiburg E. Miscible rectilinear displacements with gravity override, Part 1, Homogeneous porous medium. *Journal of Fluid Mechanics* 2000; **420**:225–257.
17. Singh B, Azaiez J. Numerical simulation of viscous fingering of shear-thinning fluids. *Canadian Journal of Chemical Engineering* 2001; **79**:961–967.
18. Moissis DE, Miller CA, Wheeler MF. A parametric study of viscous fingering in miscible displacement by numerical simulation. In *Numerical Simulation in Oil Recovery*, vol. 11. Wheeler MF (ed.). 1988; 227–247.
19. Coutinho ALGA, Alves JLD. Finite element simulation of nonlinear viscous fingering in miscible displacements with anisotropic dispersion and nonmonotonic viscosity profiles. *Computational Mechanics* 1999; **23**:108–116.
20. Coutinho ALGA, Dias CM. Stabilized finite element methods with reduced integration techniques for miscible displacements in porous media. *International Journal for Numerical Methods in Engineering* 2004; **59**: 475–492.
21. Castro RGS, Malta SMC, Loula AFD, Landau L. Numerical analysis of space-time finite element formulations for miscible displacements. *Computational Geosciences* 2001; **5**:301–330.
22. Meiburg E, Chen C-Y. High-accuracy implicit finite-difference simulations of homogeneous and heterogeneous miscible-porous-medium flows. *Society of Petroleum Engineers Journal* 2000; **5**(2):129–137.
23. Hill S. Channelling in packed columns. *Chemical Engineering Science* 1952; **1**:247–253.
24. Tchelepi HA. Viscous fingering, gravity segregation and permeability heterogeneity in two-dimensional and three-dimensional flows. *Ph.D. Thesis*, Department of Chemical Engineering, Stanford University, U.S.A., 1994.
25. Bracewell RN, Benuman O, Hao H, Villasenor J. Fast two-dimensional Hartley transform. *Proceedings of the IEEE* 1986; **74**(9):1283–1284.
26. Bracewell RN. *The Hartley Transform.* Oxford University Press: Oxford, 1986.
27. Canuto C, Hussaini MY, Quarteroni A, Zang TA. *Spectral Methods in Fluid Dynamics.* Springer-Verlag: New York, 1987.
28. Peaceman DW, Rachford Jr HH. The numerical solutions of parabolic and elliptic differential equations. *SIAM Journal* 1955; **3**:28–41.
29. Ferziger JH. *Numerical Methods for Engineering Application.* Wiley: New York, 1981.
30. Lele SK. Compact finite difference scheme with spectral-like resolution. *Journal of Computational Physics* 1992; **103**:16–42.
31. Kawaguchi M, Makino K, Kato T. Comparison of viscous fingering patterns in polymer and Newtonian fluids. *Physica D* 1997; **105**(1–3):121–129.
32. Li H. Viscous fingering in non-Newtonian flow. *M.Sc. Thesis*, Department of Chemical & Petroleum Engineering, University of Calgary, Canada, 2002.

